Microporous and Mesoporous Materials 131 (2010) 303–309

Contents lists available at ScienceDirect

Microporous and Mesoporous Materials

journal homepage: www.elsevier.com/locate/micromeso

Preparation and performance of straw based activated carbon for supercapacitor in non-aqueous electrolytes

Xueliang Li *, Changlong Han, Xiangying Chen, Chengwu Shi

School of Chemical Engineering, Anhui Key Laboratory of Controllable Chemistry Reaction and Material Chemical Engineering, Hefei University of Technology, Hefei, Anhui 230009, PR China

ARTICLE INFO

Article history:
Received 23 June 2009
Received in revised form 28 December 2009
Accepted 11 January 2010
Available online 14 January 2010

Keywords:
Activated carbon
EDLCs
Organic electrolytes
Specific surface area
Accessible volume

ABSTRACT

The activated carbon with honeycomb-like morphology for electrochemical double layer capacitors (EDLCs) was prepared from wheat straw by carbonization and subsequent activation with KOH. The product presented micro- and mesoporous structure with the peak pore size of 2.1 nm and high specific surface area of 2316 m^2/g. The electrochemical capacitance performances of the activated carbon as EDLC electrodes were characterized by using cyclic voltammetry (CV), alternating current (AC) impedance. The specific capacitance of the activated carbon reached 251.1 F/g at 2 mV/s scan rate in the electrolyte of $MeEt_3NBF_4$/AN. The thermal gravimetric analysis of AN impregnated carbon was explored as a new approach to investigate the effectivity of pore for the electrolytes. The relationships between specific capacitance and scan rate, surface area and pore diameter were discussed.

1. Introduction

Supercapacitors have wide applications in many fields, such as hybrid electric vehicles, energy storage systems and memory back-up. They have attracted much attention due to their high power and high capacitance compared with batteries and traditional capacitors, respectively. They have been used to improve the performance and service life of batteries and fuel cells.

Owing to the advantages of high specific area, low cost, good stability etc., activated carbon has attracted extensive researches [1–4] as an important electrode material. Naturally, raw materials affect the formation mechanism and specific surface area of activated carbon [5], and much work has been done on coal-based carbon [6–9] and resin-based carbon [10–12]. In addition, other raw materials, such as shells [13–16], olive-seed waste residues [17], banana fibers [18], were also used as carbon source to prepare activated carbon for EDLCs.

Obviously, as a kind of renewable resource, straw is cheap and easy to collect. The straw has natural plant fiber structure and this structure may provide an opportunity to prepare activated carbon with high specific capacitance. However, there are few reports on the preparation of activated carbon for EDLCs from straw.

Compared with the electrochemical stability, activated carbon has wider potential window in organic electrolytes than in aqueous ones. Hence the electrode materials could present high energy density. For electrode materials of EDLCs in organic electrolytes, much work has been done on preparation of electrode materials and the improvement of capacitance performance. Taberna et al. [19] have done researches on the assembly of composite electrodes from activated carbon and carbon nanotube, and obtained the carbon material with specific capacitance of 88 F/g in NEt_4BF_4/AN electrolyte. Activated carbons [7] from petroleum-based needle coke exhibited specific surface areas from 400 to 2900 m^2/g, specific capacitances of 14–44 F/g. The performances of high temperature carbon–carbon supercapacitor [20] have been explored in ionic liquid electrolyte, and the microporous activated carbon exhibited a specific capacitance of 60 F/g and a high cycling stability. Simon and Gogotsi [21] reported the double layer capacitance of activated carbon reached 100–120 F/g in organic electrolytes in their latest review article. By means of solidification, carbonization and chemical activation with KOH, gelatin-based porous carbon beads [22] were fabricated, and the carbon material exhibited good specific capacitance of 119.8 F/g in Et_4NBF_4/AN electrolyte.

Some work [8,14,23] focused on the research of the relation between specific capacitance and pore structure. Blanco et al. [23] investigated the accessibility of the electrolyte to the micropores using carbon molecular sieves as the model of preparing active electrode materials. However, to improve the capacitance performance, further research is necessary and will be benefit to understand pore utility at different scan rates.

Gogotsi and co-workers investigated the carbide-derived carbon (CDC) for supercapacitors and achieved the capacitance of 90–145 F/g with the current density of 5–100 mA/cm^2 in

* Corresponding author. Tel.: +86 551 2904030; fax: +86 551 2901450.
E-mail address: xueliangli2005@163.com (X. Li).

1387-1811/$ - see front matter © 2010 Elsevier Inc. All rights reserved.
doi:10.1016/j.micromeso.2010.01.007

Et_4NBF_4/AN [24]. After chemical activation of CDC with KOH, capacitance value in an organic electrolyte leads to 180 F/g [25]. For this tendency of the capacitance change, the activation step plays an important role in preparation of activated carbon used in EDLCs. And we have paid attention to this key step in the study.

In the work, wheat straw based activated carbon was successfully prepared for organic electrolyte EDLCs. The high capacitance of 251.1 F/g was obtained in organic electrolytes. The carbonization behavior and surface morphology of activated carbon were studied. The pore structure and capacitance performances were investigated, and the relation between them was analyzed to further understand the role of pore size in forming capacitance. Accessible volume to solution was determined via the mass loss of the carbon impregnated by AN, and the minimal diameter of effective pore was obtained.

2. Experimental

2.1. Preparation of wheat straw based activated carbon

Activated carbon for EDLCs in organic electrolytes was prepared from wheat straw. The wheat straw was crushed and sieved to particle sizes ranging from 0.6 to 1.0 mm, then carbonized at 420 °C for 120 min. Carbonized samples were washed with distillated water, dried and added into KOH solution. The weight ratio of carbonized samples to KOH was 1:3.5 in the mixed system. The system was stirred for 60 min and then dried in the oven at 110 °C. The activation of the carbonized samples was performed in the furnace at 700 °C for 120 min. After cooled down, the mixture was washed with distilled water for several times to remove residual KOH and by-products. Finally, straw based activated carbon was obtained after drying at 140 °C for 240 min.

2.2. Characterizations of wheat straw based activated carbon

Thermal gravimetric analysis (TGA) of wheat straw was carried out on a Shimadzu TA-50H thermal analyser at a heating rate of 7 °C/min in flowing nitrogen, increasing from 24 °C to 550 °C to investigate the decomposition course of wheat straw. The morphologies of the as-prepared activated carbon were observed on Hitachi (X-650) scanning electron microanalyzer. Nitrogen adsorption isotherms were obtained at 77 K using Micrometrics ASAP 2020. The specific surface area was determined by the BET equation and pore size distribution was calculated with the adsorption data based on original density functional theory.

The electrochemical measurement was carried out by cyclic voltammetry and AC impedance on an electrochemical workstation CHI660B. The electrode slurry was fabricated by mixing activated carbon powders, acetylene black and polyvinylidene fluoride (PVDF) with a weight ratio of 7:2:1 in *N*-methyl-2-pyrrolidone (NMP), and the resultant slurry was coated onto an aluminum foil. Then the electrode was obtained by drying at 80 °C for 12 h under vacuum. After electrodes and paper separator were pre-impregnated with electrolyte of 1.2 mol/L $MeEt_3NBF_4$/propylene carbonate (PC) or 1.2 mol/L $MeEt_3NBF_4$/acetonitrile (AN), EDLCs were assembled by sandwiching the paper separator between two electrodes, and then pressing them tightly. The EDLCs were fabricated in a dry glove box filled with high purity argon gas. Cyclic voltammetry was conducted from −2 V to 2 V at different scan rates in electrolytes of $MeEt_3NBF_4$/PC or $MeEt_3NBF_4$/AN. The specific capacitance of the as-prepared activated carbon can be obtained from CV curves using the Eq. (1):

$$C = 2\Delta I/(v \cdot m) \quad (1)$$

where v and m denote potential scan rate (mV/s), the total mass of the active material (g) in two electrodes (the mass of each electrode material is same), and ΔI and C denote the difference between cathodic current and anodic one (mA), and the specific capacitance per unit mass of active material in the electrode (F/g). The AC impedance spectrum was measured over the frequency ranging from 0.1 Hz to 100,000 Hz with AC potential amplitude of 5 mV.

3. Results and discussion

3.1. Carbonization behavior and surface morphology

Thermogravimetric analysis for wheat straw was shown in Fig. 1. The TGA curve showed that the straw started to decompose at about 260 °C, which could explain fuming in the decomposition course at the same temperature. The straw rapidly decomposed with the increase of temperature and decomposition reaction mainly took place below 320 °C. With the further increase of temperature, decomposition reaction continued. The weight loss reached about 60% at 400 °C, which was close to the theoretical value of carbon in carbohydrate. When temperature exceeded 400 °C, the mass slowly decreased with a constant rate due to tiny particle carbon escaping from the sample. Considering complete carbonization of straw at 420 °C, we chose this temperature as the carbonization temperature of wheat straw in the preparation of carbonized samples.

Fig. 2 showed the representative SEM images of wheat straw based activated carbon obtained at 700 °C for 120 min. The experimental condition was chosen referring to our patent CN 101037200A [26]. Honeycomb-like morphology and lots of nano holes were found on the surface in Fig. 2(a). Detailed observation on the sample in Fig. 2(b) revealed that activated carbon was comprised by a large number of pores with a uniform size distribution. Both mesopores and micropores formed channels with different sizes useful for electrolyte transfer. Fig. 2 indicated that the activation process took place on the surface of pore. Molten KOH covered and permeated through the surface of carbonized samples. The reaction continued on interface and formed small pores. With the time increasing, the small ones gradually became larger and resulted in the formation of activated carbon with semi-sphere pores.

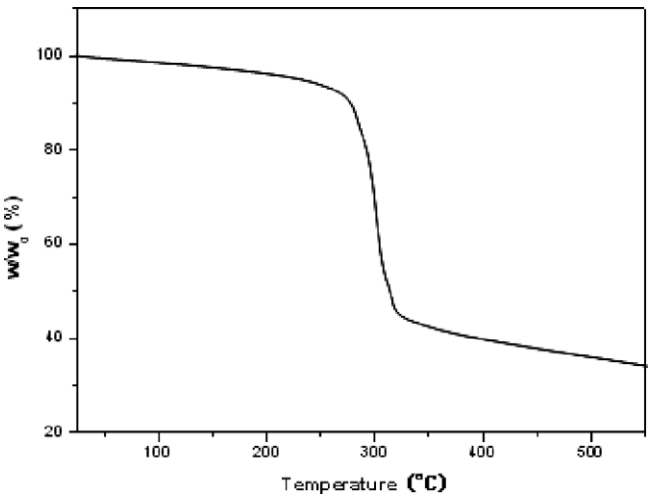

Fig. 1. TGA curve of wheat straw powder.

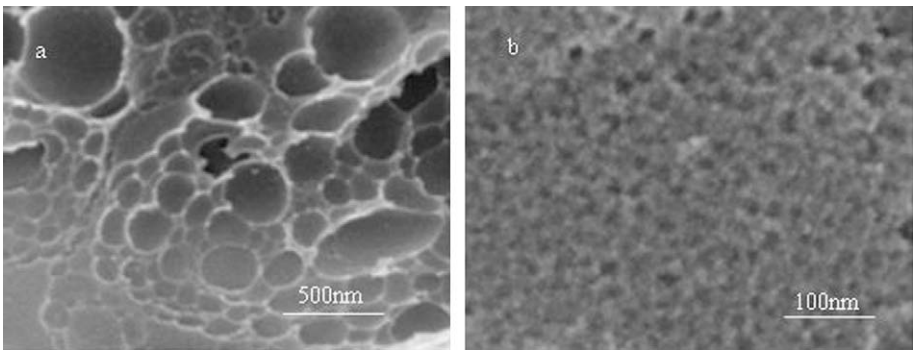

Fig. 2. SEM images of the activated carbon prepared at 700 °C for 120 min in different magnification.

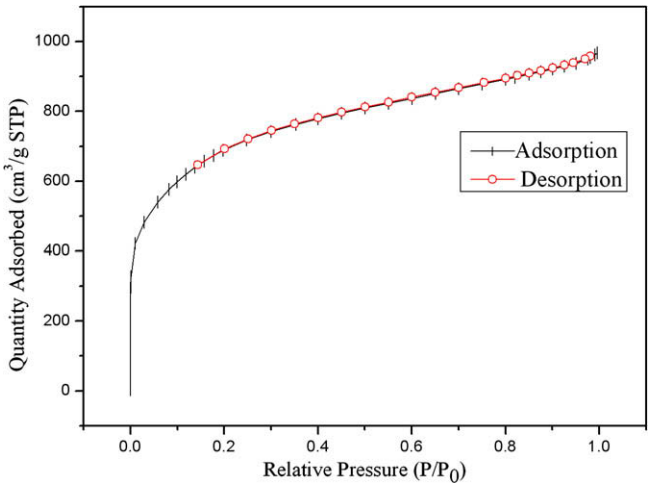

Fig. 3. Nitrogen adsorption–desorption isotherm at 77 K for the as-prepared activated carbon.

3.2. Pore structure

Activated carbon presented complex porous structure. Further information on pore structure could be obtained from nitrogen adsorption–desorption isotherm as shown in Fig. 3. Adsorption steeply increased at low relative pressure, suggesting the presence of a large number of micropores. The pore size distribution was exhibited in Fig. 4. The maximum peak of the as-prepared activated carbon could be found at 2.1 nm in Fig. 4(a). The sizes of pores were almost in the range of 0.4–10 nm. The BET surface area and total pore volume from the nitrogen adsorption isotherm reached 2316 m^2/g and 1.496 cm^3/g, respectively.

The cumulative pore volume increased quickly with the decrease of pore width. Although the pores with width less than 0.5 nm had large specific surface area, electrolytes were hard to access to the surface inside small pores and these narrow pores did not contribute to double layer capacitance. For all the pores larger than 3.5 nm, the sum of specific surface area was only 89 m^2/g. So for EDLCs, the pores in the range of 0.5–3.5 nm provided mainly specific surface area in forming double layer capacitance. As shown in Fig. 4(b), the value of dV/dr almost remained constant in the range of 0.4–3.5 nm.

The relationship between cumulative surface area and pore width was obtained from Fig. 5 and for the pores with width less than 3.5 nm, it could be expressed by following equation:

$$S = 2636 - 1703\lg D \quad (2)$$

This linear relation of S vs. $\lg D$ was determined by the special pore structure of the activated carbon and the pore structure should explain the Eq. (2). Based on the nitrogen adsorption–desorption isotherm, we made the following analysis. The relation of volume and the pore size for semi-sphere structure could be represented as $dV = f(r) \cdot 2/3 \cdot \pi \cdot r^3\, dr$, where $f(r)$ is the function related to pore size. Considering the constant value of dV/dr, $f(r)$ could be expressed as $f(r) = k_1/r^3$.

The specific surface area of the as-prepared activated carbon increased with the decrease of pore diameter. Considering the semi-sphere surface, this could be written as

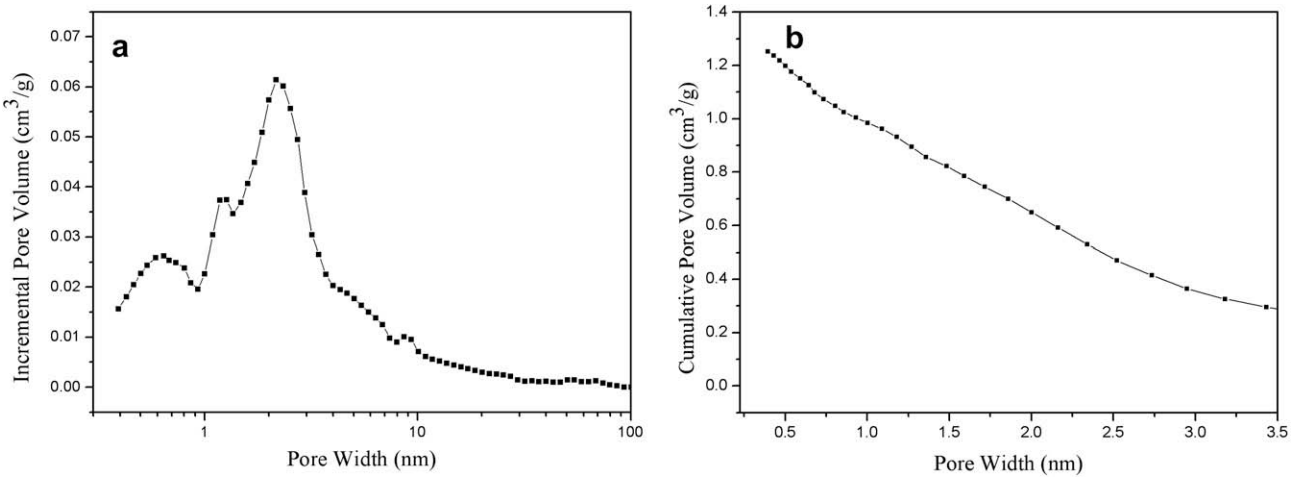

Fig. 4. (a) Incremental pore volume and (b) cumulative pore volume vs. pore width for the as-prepared activated carbon.

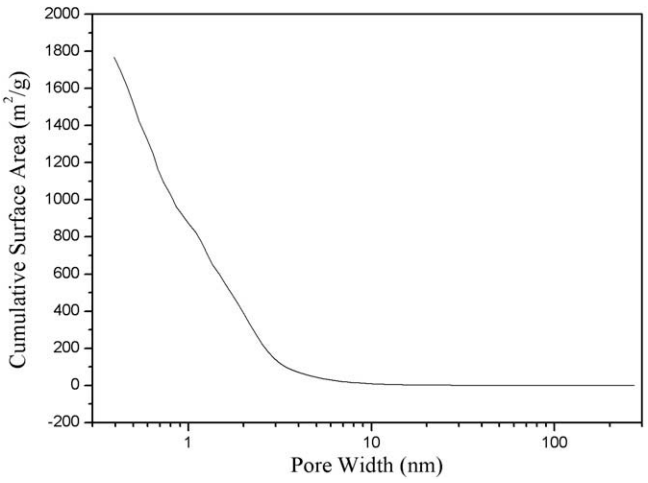

Fig. 5. Cumulative surface area vs. pore width for the activated carbon.

$$S - S(r_m) = \int_r^{r_m} f(r)2\pi r^2 dr = 2\pi k_1 \ln(r_m/r) = 2\pi \ln 10 k_1 (\lg D_m - \lg D) \quad (3)$$

where S is specific surface area of activated carbon (m^2/g), D is diameter of pore (nm), k_1 is coefficient, D_m is upper limit where the linear relation of S vs. lg$D$ can maintain. The Eq. (3) describes the relation of specific surface area and pore diameter from theoretical aspect.

3.3. Capacitance performances

Fig. 6 presented cycle voltammetry curves of EDLCs made by the activated carbon at different scan rates at room temperature. Fig. 6a and b corresponded to the electrolytes of $MeEt_3NBF_4$/PC and $MeEt_3NBF_4$/AN, respectively. It could be seen from Fig. 6A that the shape of CV curves at the cathode and the anode processes were symmetric. The shape of CV curves in Fig. 6B is similar to Fig. 6A. These results revealed that the activated carbon exhibited capacitance performance in organic electrolytes, both on positive potential and negative potential. The shape of curves became more rectangular with the decrease of scan rate and the voltammetric currents increased with the increase of scan rate. The results implied that, for small potential scan rate, electrolytes had enough time to enter into micropores, and micropores were effectively used for forming double layer capacitance.

The specific capacitances of the as-prepared activated carbon in the electrolytes of $MeEt_3NBF_4$/PC and $MeEt_3NBF_4$/AN were shown in Fig. 7. The values at different potentials were calculated by Eq. (1) and were almost the same in the range of −1.5–1.5 V. In the following discussion, specific capacitances at different scan rates were given at the potential of 0.0 V. The data of activated carbon is 236.4 F/g at a scan rate of 2 mV/s in the electrolyte of $MeEt_3NBF_4$/PC. The value in $MeEt_3NBF_4$/AN is higher than that in $MeEt_3NBF_4$/PC. The corresponding specific capacitance reaches 251.1 F/g at a scan rate of 2 mV/s in $MeEt_3NBF_4$/AN electrolyte. It may be attributed to the difference of the solvent molecular sizes. Compared with AN, solvent PC with larger molecular size was hard to access to micropores, causing the decrease of specific capacitance. The value of the as-prepared activated carbon increased with the decrease of scan rate. There was a linear relation between the specific capacitance of activated carbon and the logarithm of scan rate and the following equation was fitted from the data in Fig. 7.

$$C = 259 - 68 \lg v \quad (4)$$

Fig. 8 gave Nyquist plots of EDLCs in organic electrolytes and showed the impedances corresponding to the frequency of 0.1–100,000 Hz. Generally speaking, the impedances in high frequency region were mainly determined by the total resistance including reactive resistance, electrolyte resistance and activated carbon resistance. It could be seen that the resistance of EDLCs in $MeEt_3NBF_4$/AN electrolyte was 0.62 Ω and the resistance of ones in $MeEt_3NBF_4$/PC electrolyte was 1.63 Ω. The former was smaller than the latter owing to that $MeEt_3NBF_4$/AN had lager conductance. For the ideal EDLCs [27], the imaginary part of the impedance spectra at low frequencies approached to a vertical line suggesting a capacitive behavior. Obviously, Nyquist plots at low-frequency parts inclined. This phenomenon may be due to the fact that the electrolytes entered into micropores and caused the increase of electrolyte ions diffusion resistance.

3.4. Role of pore size in forming capacitance

The capacitance of electrical double layer comes from attributions of electrochemically available interface of electrode/electrolyte. Hence, the total capacitance was the sum of capacitance with different pore structures and sizes. The specific capacitance

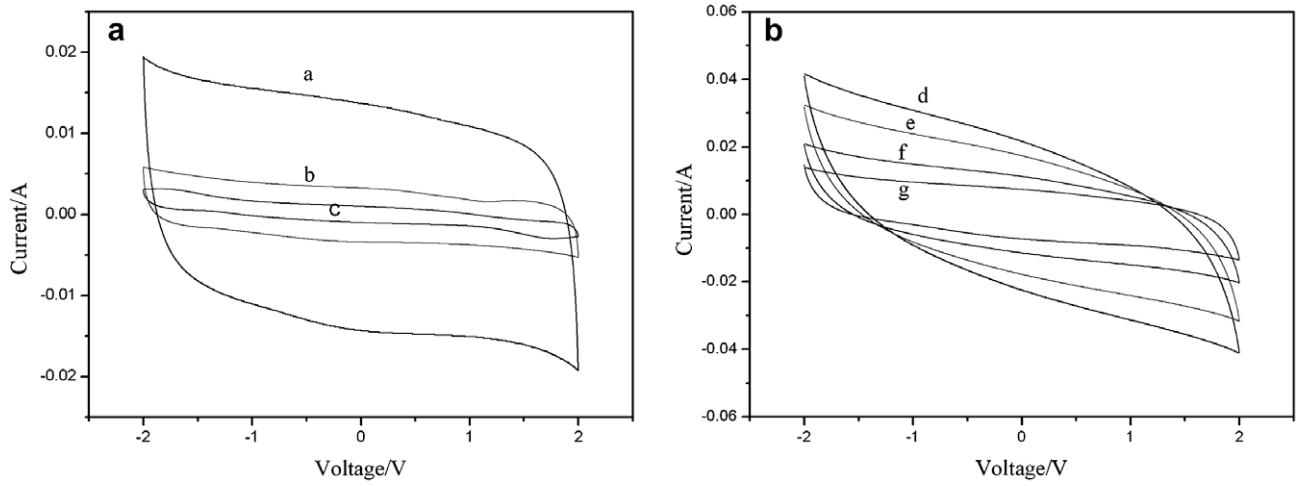

Fig. 6. Cycle voltammetry curves of EDLCs made by wheat straw based activated carbon at different scan rates at room temperature, (a) $MeEt_3NBF_4$/PC, 50 mV/s; (b) $MeEt_3NBF_4$/PC, 10 mV/s; (c) $MeEt_3NBF_4$/PC, 2 mV/s; (d) $MeEt_3NBF_4$/AN, 300 mV/s; (e) $MeEt_3NBF_4$/AN, 200 mV/s; (f) $MeEt_3NBF_4$/AN, 100 mV/s; (g) $MeEt_3NBF_4$/AN, 50 mV/s.

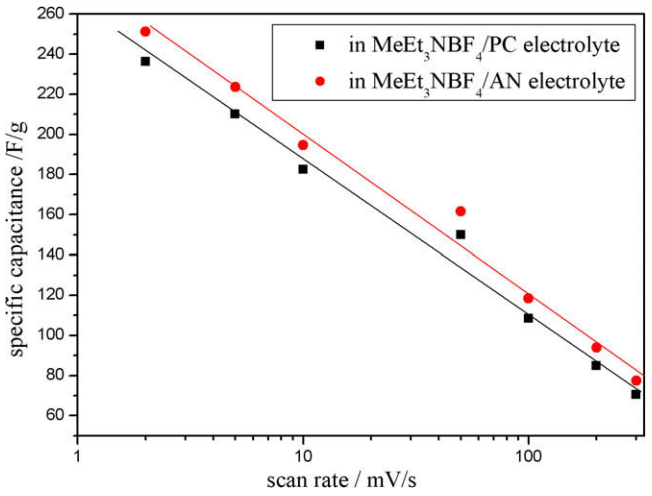

Fig. 7. The relationship between specific capacitance of wheat straw based activated carbon and scan rate in the electrolytes of $MeEt_3NBF_4$/PC and $MeEt_3NBF_4$/AN.

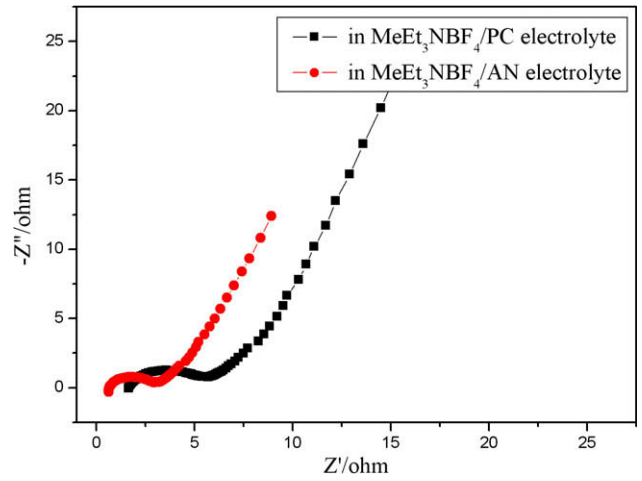

Fig. 8. AC impedance of EDLCs made by wheat straw based activated carbon in the electrolytes of $MeEt_3NBF_4$/PC and $MeEt_3NBF_4$/AN at room temperature.

of activated carbon for semi-sphere pores could be described as follows:

$$C = \int_{r_0}^{r_m} k_1/r^3 \times C_m \times 2\pi r^2 dr = 2\pi k_1 C_m \ln 10 \times (\lg D_m - \lg D_0) \quad (5)$$

where C_m and k_1 were real capacitance per unit area and coefficient, respectively. The Eq. (5) describes the relation of specific capacitance and pore diameter from theoretical aspect.

The capacitance per surface area can be obtained from the calculation of capacitance divided by total area. The values of carbon materials were discussed in organic electrolytes ranging from 0.06 F/m^2 to 0.35 F/m^2 in some Refs. [13,28,29]. For the present activated carbon, the value was 0.103 F/m^2 and was coincident with the reported value.

Owing to ineffective utility of very narrow pores (non-accessible pores by electrolytes), the available surface area became small and the real capacitance per unit area was higher than the apparent one. Combining Eq. (2) and C_m, the relation of the specific capacitance and pore width was calculated as follows:

$$C = (2636 - 1703 \lg D) \times C_m \quad (6)$$

The pores larger than 0.8 nm could efficiently form double layers for organic electrolyte [9]. So we choose the diameter (D) of 0.80 and 0.90 nm, and calculate the real capacitance per unit area (C_m) from Eqs. (6) and (4). For the scan rate of 2 mV/s, the capacitance (C) calculated from Eq. (4) is 238.53 F/g. And then the real C_m were 0.217 and 0.236 F/m^2 for D of 0.80 and 0.90 nm, respectively.

It is well known that the pore with width larger than the diameter of electrolyte could be utilized to form double layer capacitance. So the real capacitance per unit area was ca. 0.23 F/m^2 for the present activated carbon.

3.5. TGA of AN impregnated carbon and effective pore analysis

Nitrogen adsorption–desorption isotherm could provide the important pore structure information and can be applied effectively for the substances with the almost same size of N_2 molecule. For the substances with the other size, nitrogen adsorption–desorption isotherm could provide valuable guidance to analyze pore structure in some extent. Owing to the fact that the size of solvent AN molecule is larger than that of N_2, not all the pores of activated carbon can be filled by AN, hence only partial surface could be utilized to form capacitance. Here, we employed TGA as a new approach to investigate the impregnated state of activated carbon with electrolyte solution. It may provide the opportunity to characterize structures and the minimal size of effectively utilized pore of activated carbon impregnated by AN.

The mass loss resulted from liquid evaporation and desorption of adsorbed substance, and the loss amount could be measured by TGA curves. The total adsorbed volume may be sum of all accessible volume of pores for solution. Fig. 9 showed mass loss curves of activated carbon impregnated by AN, and corresponding derivative curves were given in the inserts. It could be seen from Fig. 9 that the mass loss process displayed three stages, and Fig. 10 illustrated the three stages of AN evaporation from AN impregnated porous carbon.

During the first stage in Fig. 9 (from beginning to ca. 50 min), the rapid decrease in mass of sample was showed in the mass loss curves. The decline presented a constant rate, and it was confirmed from the horizontal line in the plot of dm/dt vs. time. This phenomena was attributed to the AN vaporization outside of pores (see in Fig. 10).

In the second stage in Fig. 9 (from ca. 50 min to the time of "D" point), the evaporation rate of solvent gradually decreased. It corresponded to the evaporation of solvent between carbon particles (see in Fig. 10). Owing to larger evaporation resistance of solvent

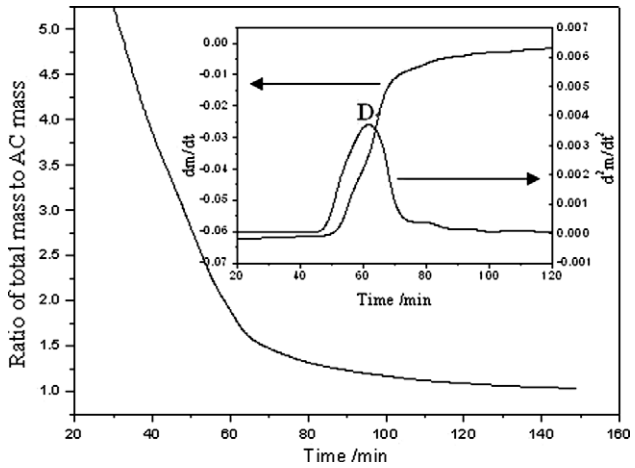

Fig. 9. Mass loss curves at 65 °C and derivative curves (the inserts) for AN impregnated activated carbon prepared at conditions of 700 °C, 120 min.

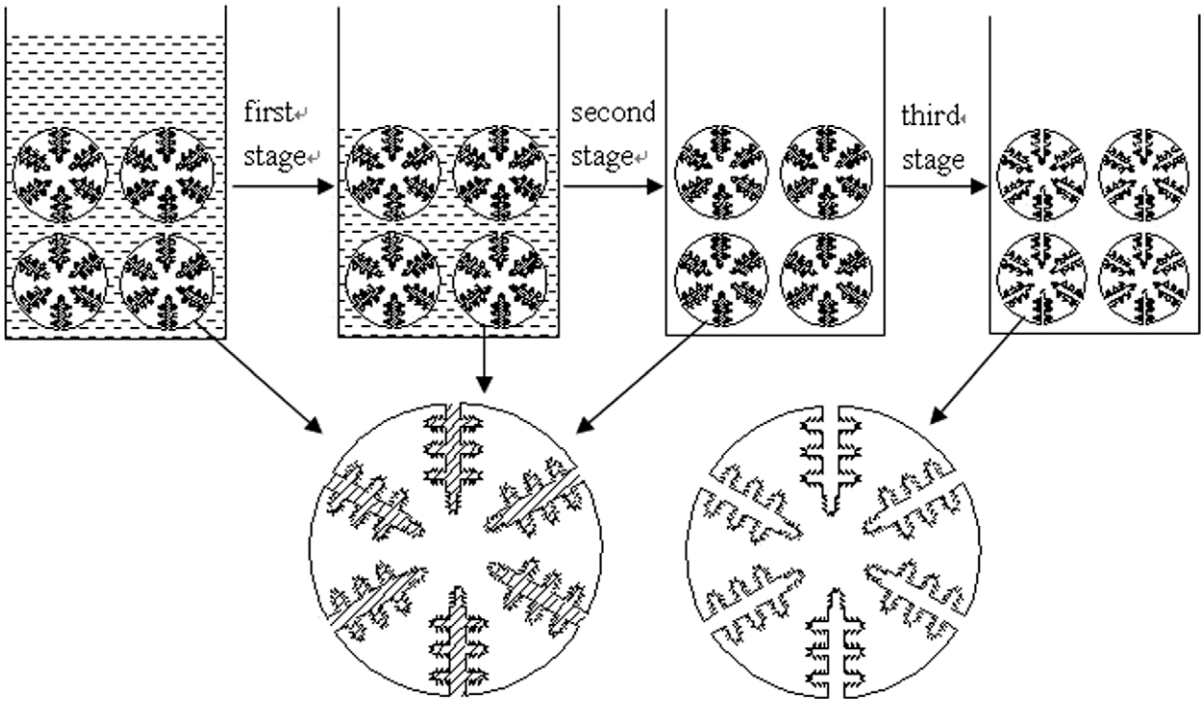

Fig. 10. Schematic diagram of mass loss process from AN impregnated porous carbon.

between carbon particles, the evaporation rate was smaller than that in first stage.

The "*D*" gave the max second order derivative value in the plot of d^2m/dt^2 vs. time, and this critical point became the boundary between the second stage and the third one, when the AN between particles were vaporized completely and afterwards the AN in the pores began to vaporize (see in Fig. 10). It may show the distinct difference of mass loss between the second stage and the third stage.

In the third stage in Fig. 9 (the time after "*D*"), the rate of mass loss further became small, the process of the solvent in pores vaporized was desorption of the solvent from pores (see in Fig. 10). The rate became small as the process continued owing to the big diffusion resistance and small evaporation propulsion (The smaller the pore is, the smaller the equilibrium vapor pressure will be.).

We can see from Fig. 9 that 0.8 g AN impregnated pores and surfaces of 1 g activated carbons at activated temperature of 700 °C. The desorption volume of AN per unit activated carbon in the third stage was 1.02 mL/g. According to N_2 adsorption result of cumulative volume vs. pore width, the accessible volume of 1.02 mL/g was the sum of all volumes of pores larger than 0.85 nm from Fig. 4. So minimal pore width for AN access was 0.85 nm and larger pores could be impregnated by AN and provide double layer capacitance. The result from the TGA of AN impregnated porous carbon showed that the pores larger than 0.85 nm could form effective double layers. The method could be also used to analyze the surface impregnated state of porous materials and capacitance performance.

4. Conclusion

The straw based activated carbon for EDLCs in organic electrolytes was prepared by carbonization and subsequent activation with KOH. The presence of micropores and mesopores made the specific area reaching 2316 m^2/g which could form high double layer capacitance. The specific capacitance reached 251.1 F/g at a scan rate of 2 mV/s in $MeEt_3NBF_4$/AN electrolyte. The pores larger than 0.85 nm could be impregnated by electrolytes and formed effective capacitance. The specific capacitance of the activated carbon was linear function with the logarithm of scan rate. And the specific area and the logarithm of pore diameter exhibited linear relation when the pore diameter was less than 3.5 nm.

Acknowledgment

This work was financially supported by the 2007 Annual Key Project of Anhui Province of China (Nos. 07020203003) and (08020203005).

References

[1] R. Pietrzak, K. Jurewicz, P. Nowicki, K. Babel, H. Wachowska, Fuel 86 (2007) 1086.
[2] M.J. Bleda-Martinez, D. Lozano-Castello, E. Morallon, D. Cazorla-Amoros, A. Linares-Solano, Carbon 44 (2006) 2642.
[3] M.J. Bleda-Martinez, J.A. Macia-Agullo, D. Lozano-Castello, E. Morallon, D. Cazorla-Amoros, A. Linares-Solano, Carbon 43 (2005) 2677.
[4] J. Li, J. Li, Y.Q. Lai, H.S. Song, Z.A. Zhang, Y.X. Liu, J. Cent. South Univ. Technol. 13 (2006) 360.
[5] G.G. Stavropoulos, Fuel Process. Technol. 86 (2005) 1165.
[6] Q. Li, K.X. Li, F.R. Wang, G.H. Sun, New Carbon Mater. 20 (2005) 335.
[7] W.M. Qiao, S.H. Yoon, I. Mochida, Energy Fuels 20 (2006) 1680.
[8] G. Gryglewicz, J. Machnikowski, E. Lorenc-Grabowska, G. Lota, E. Frackowiak, Electrochim. Acta 50 (2005) 1197.
[9] E. Raymundo-Pinero, K. Kierzek, J. Machnikowski, F. Beguin, Carbon 44 (2006) 2498.
[10] F.R. Wang, K.X. Li, Y.G. Lu, Q. Li, C.X. Lu, C.G. Sun, New Carbon Mater. 21 (2006) 219.
[11] L.H. Wang, M. Fujita, M. Inagaki, Electrochim. Acta 51 (2006) 4096.
[12] S.I. Lee, S. Mitani, C.W. Park, S.H. Yoon, Y. Korai, I. Mochida, J. Power Sources 139 (2005) 379.
[13] D. Hulicova, M. Kodama, H. Hatori, Chem. Mater. 18 (2006) 2318.
[14] F.C. Wu, R.L. Tseng, C.C. Hu, C.C. Wang, J. Power Sources 144 (2005) 302.
[15] P.W. Zhou, B.H. Li, F.Y. Kang, Y.Q. Zeng, New Carbon Mater. 21 (2006) 125.
[16] Y.P. Guo, J.R. Qi, Y.Q. Jiang, S.F. Yang, Z.C. Wang, H.D. Xu, Mater. Chem. Phys. 80 (2003) 704.
[17] G.G. Stavropoulos, A.A. Zabaniotou, Micropor. Mesopor. Mater. 82 (2005) 79.
[18] V. Subramanian, C. Luo, A.M. Stephan, K.S. Nahm, S. Thomas, B.Q. Wei, J. Phys. Chem. C 111 (2007) 7527.
[19] P.L. Taberna, G. Chevallier, P. Simon, D. Plee, T. Aubert, Mater. Res. Bull. 41 (2006) 478.

[20] A. Balducci, R. Dugas, P.L. Taberna, P. Simon, D. Plee, M. Mastragostino, S. Passerini, J. Power Sources 165 (2007) 922.
[21] P. Simon, Y. Gogotsi, Nat. Mater. 7 (2008) 845.
[22] Y. Ci, J. Ge, X.F. Wang, W.H. Chen, Y.C. Guo, L.J. Chen, Chin. J. Inorg. Chem. 23 (2007) 365.
[23] V. Ruiz, C. Blanco, R. Santamaria, J.M. Juarez-Galan, A. Sepulveda-Escribano, F. Rodriguez-Reinoso, Micropor. Mesopor. Mater. 110 (2008) 431.
[24] J. Chmiola, G. Yushin, Y. Gogotsi, C. Portet, P. Simon, P.L. Taberna, Science 313 (2006) 1760.
[25] C. Portet, M.Á. Lillo-Ródenas, A. Linares-Solano, Y. Gogotsi, Phys. Chem. Chem. Phys. 11 (2009) 4943.
[26] X. Li, C. Han, Y. Luo, C. Shi, X. Chen, Chinese Patent CN 101037200A, 2007, p. 9.
[27] B.E. Conway, Electrochemical Supercapacitors: Scientific Fundamentals and Technological Applications, Kluwer–Plenum Press, New York, 1999.
[28] O. Barbieri, M. Hahn, A. Herzog, R. Kotz, Carbon 43 (2005) 1303.
[29] M. Sevilla, S. Alvarez, T.A. Centeno, A.B. Fuertes, F. Stoeckli, Electrochim. Acta 52 (2007) 3207.